APPENDIX A: SPECIFIC INFORMATION FOR SAR COMPUTATIONS

This appendix provides additional details on simulations and the computational code. Most of the information regarding the code employed to perform the numerical computations has been adapted from the standard IEC/IEEE 62704-2:2017 and from the XFDTD™ User Manuals. Remcom Inc., owner of XFDTD™, is kindly acknowledged for the help provided.

1) Computational resources

a) A multiprocessor system equipped with two Intel Xeon E5-2697 v3 14-core CPUs and four NVIDIA Tesla K40 GPUs was employed for all simulations.

b) The memory requirement was from 7 GB to 20 GB. Using the above-mentioned system with 28-cores operating concurrently, the typical simulation would run for 6-10 hours and with all four GPUs activated by the XFDTD version 7.6 this time would be from 60-180 min.

2) FDTD algorithm implementation and validation

a) We employed a commercial code (XFDTD™ v7.6, by Remcom Inc.) that implements the Yee's FDTD formulation [1]. The solution domain was discretized according to a rectangular grid with an adaptive 3-8 mm step in all directions. Sub-gridding was not used. Seven-layer PML absorbing boundary conditions are set at the domain boundary to simulate free space radiation processes. The excitation is a lumped voltage generator with 50-ohm source impedance. The code allows selecting *wire objects* without specifying their radius. We used a wire to represent the antenna. The car body is modeled by solid metal. We did not employ the "thin wire" algorithm since within the adaptive grid the minimum resolution of 3 mm was specified and used to model the antenna and the antenna wire radius was never smaller than one-fifth of the voxel dimension. In fact, the XFDTD™ manual specifies that "In most cases, standard PEC material will serve well as a wire. However, in cases where the wire radius is important to the calculation and is less than 1/4 the length of the average cell edge, the thin wire material may be used to accurately simulate the correct wire diameter." The maximum voxel dimension in the plane normal to the antenna in all our simulations was 3 mm, and the antenna radius is always at least 1 mm (1 mm for the short quarter-wave antennas and 1.5 mm for the long gain antennas), so there was no need to specify a "thin wire" material.

Because the field impinges on the bystander or passenger model at a distance of several tens of voxels from the antenna, the details of antenna wire modeling are not expected to have significant impact on the exposure level.

b) XFDTD™ is one of the most widely employed commercial codes for electromagnetic simulations. It has gone through extensive validation and has proven its accuracy over time in many different applications. Most importantly and as required by the standard IEC/IEEE-62704-2:2017, this code has been thoroughly validated according to the standard IEC/IEEE-62704-1:2017 as described and detailed in the XFDTD™ Validation for IEC/IEEE P62704-1 report accompanying this document.

3) Computational parameters

a) The following table reports the main parameters of the FDTD model employed to perform our computational analysis:

PARAMETER	X	Y	Z
Voxel size	3-8 mm	3-8 mm	1-8 mm
Maximum domain dimensions employed for passenger computations (cells)	479	1069	671
Maximum domain dimensions employed for bystander computations (cells)	936	992	780
Time step	About 0.7 of the Courant limit (typically 5 *ps*)		
Objects separation from FDTD boundary (mm)	>200	>200	>200
Number of time steps	Defined to reach -60 dB convergence		
Excitation	Sinusoidal (not less than 10 periods)		

4) Phantom model implementation and validation

a) The human body models (bystander and/or passenger) employed in our simulations are those defined in the IEC/IEEE 62704-2-2017 standard. They are originally derived from data of the *visible human project* sponsored by the National Library of Medicine (NLM) (http://www.nlm.nih.gov/research/visible/visible_human.html). The original male data set consists of MRI, CT and anatomical images. Axial MRI images of the head and neck and longitudinal sections of the rest of the body are available at 4 mm intervals. The MRI images have 256 pixel by 256 pixel resolution. Each pixel has 12 bits of gray tone resolution. The CT data consists of axial CT scans of the entire body taken at 1 mm intervals at a resolution of 512 pixels by 512 pixels where each pixel is made up of 12 bits of gray tone. The axial anatomical images are 2048 pixels by 1216 pixels where each pixel is defined by 24 bits of color. The anatomical cross sections are also at 1 mm intervals and coincide with the CT axial images. There are 1871 cross sections. Dr. Michael Smith and Dr. Chris Collins of the Milton S. Hershey Medical Center, Hershey, Pa, created the High Fidelity Body mesh. Details of body model creation are given in the *methods* section in [2].

The final bystander and passenger model was generated for the IEC/IEEE 62704-2-2017 standard from the above dataset using the Varipose softwar, Remocm Inc., The body mesh contains 39 tissues materials. Measured values for the tissue parameters for a broad frequency range are included with the mesh data. The correct values are interpolated from the table of measured data and entered into the appropriate mesh variables.

5) Tissue dielectric parameters

a) The tissue conductivity and permittivity variation *vs.* frequency is included in the XFDTD™ calculation by a multiple-pole approximation to the Cole-Cole approximated tissue parameters reported in [6]. These parameters along with the tissue mass density values are standardized in the IEC/IEEE-62704-2:2017 standard.

6) Transmitter model implementation and validation

a) The essential features that must be modeled correctly for the particular test device model to be valid are:

- Car body. The standard car model developed and defined in the SAR computational standard IEC/IEEE 62704-2-2017 has been employed in simulations.
- Antenna. We used a straight wire, even when the gain antenna has a base coil for tuning. All the coil does is compensating for excess capacitance due to the antenna being longer than half a wavelength. We do not need to do that in the model, as we used normalization with respect to the net radiated power, which is determined by the input resistance only. In this way, we neglect mismatch losses and artificially produce an overestimation of the SAR, thereby introducing a conservative bias in the model. This simulation model was also validated by comparing the computed and measured near-field distributions in the condition with antenna mounted on the reference ground plane defined in the IEC/IEEE 62704-2-2017 standard [5].
- Antenna location. We used the same location, relative to the edge of the car trunk, the backseat, or the roof, used in the MPE measurements. Those locations are also consistent with the requirements of the IEC/IEEE 62704-2-2017 standard. The following pictures show examples of a lateral and a perspective view of the bystander and passenger model.

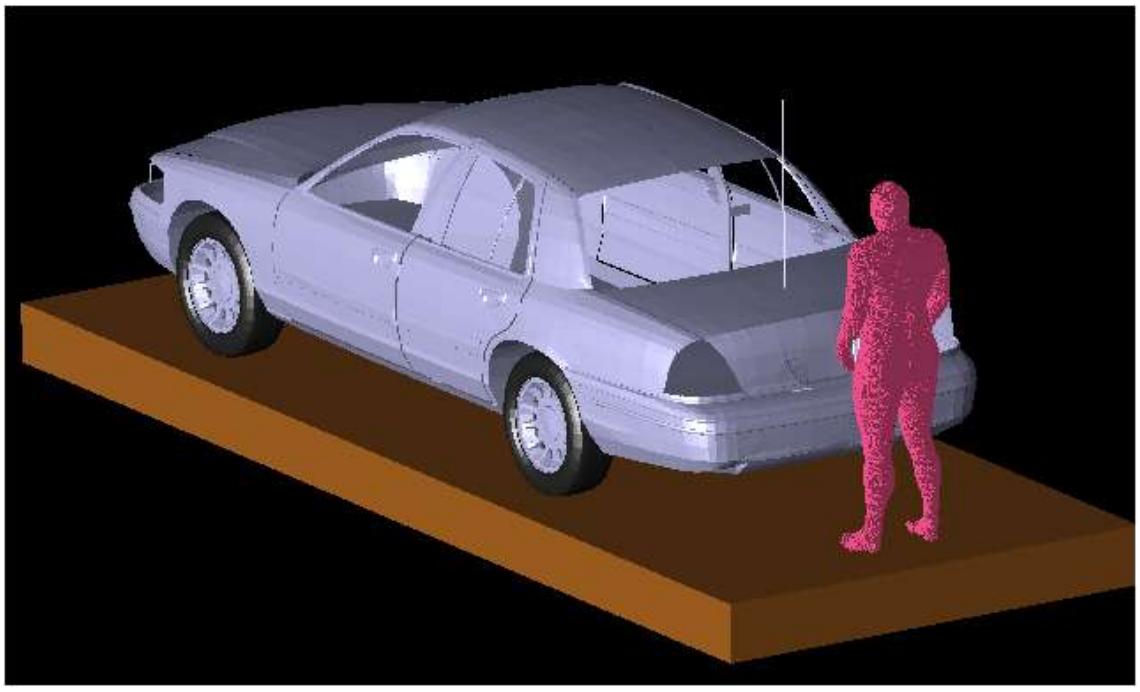

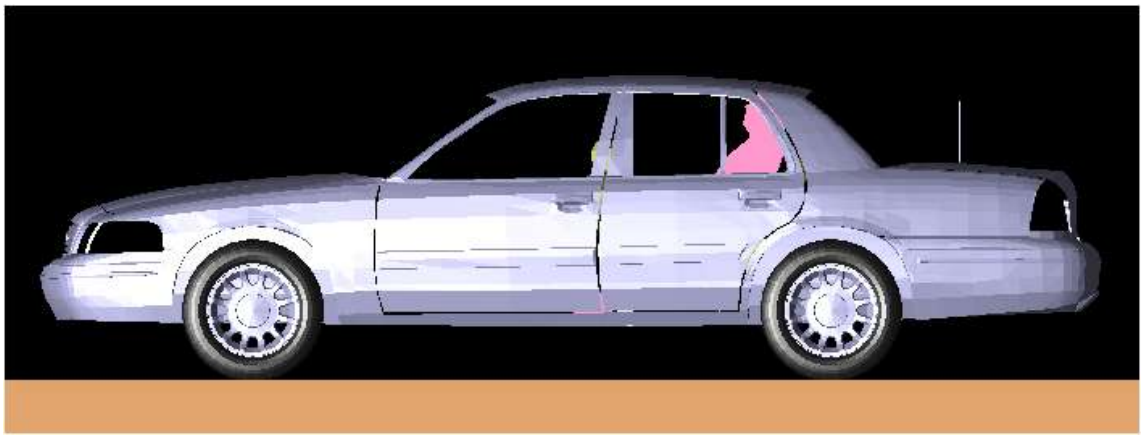

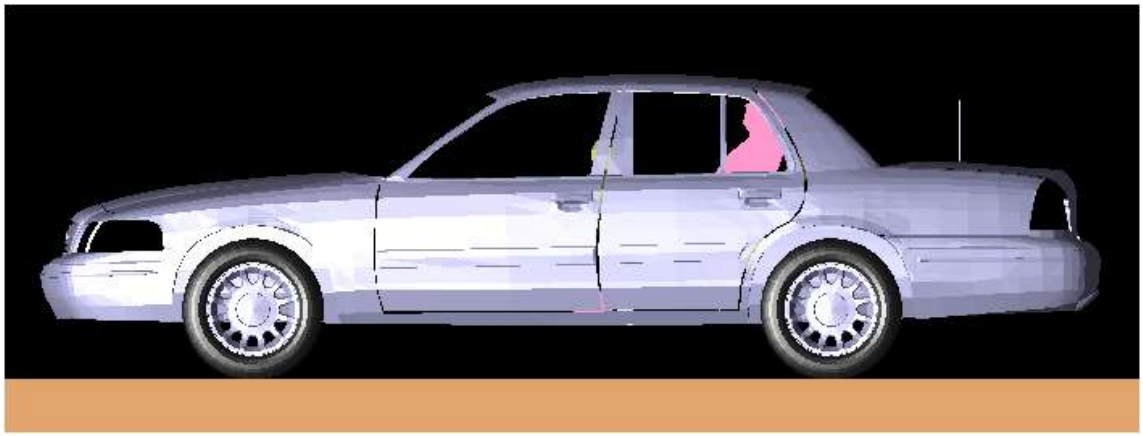

7) Test device positioning

a) A description of the device test positions used in the SAR computations is provided in the SAR report.

b) Illustrations showing the separation distances between the test device and the phantom for the tested configurations are provided in the SAR report.

8) Steady state termination procedures

a) The criteria used to determine that sinusoidal steady-state conditions have been reached throughout the computational domain for terminating the computations are based on the monitoring of field points to make sure they converge. The simulation projects were set to automatically track the field values throughout computational domain by means of XFDTD simulation control feature which ensures that "*convergence is reached when near-zone data shows a constant amplitude sine wave – when all transients have died down and the only variation left is sinusoidal. In this case "convergence" is tested on the average electric field in the space for its deviation from a pure sine wave. XFDTD automatically places points throughout the space for this purpose*." [XFDTD Reference Manual, version 7.6]. This convergence threshold was set to -60 dB.
In addition for at least one passenger and one bystander exposure condition, we placed one "field sensor" near the antenna, others between the body and the domain boundary at different locations, and one inside the head of the model. In all simulations, isotropic E-field sensors were placed at opposite sides of the computational domain. We used isotropic E and H field "sensors", meaning that all three components of the fields are monitored at these points. The following figures show an example of the time waveforms at the field point sensors in two points of the computational domain. We selected points close to antenna as well as furthest one. The highest field levels are observed for the higher index point, as it is closer to the antenna. In all cases, the field reaches the steady-state condition.

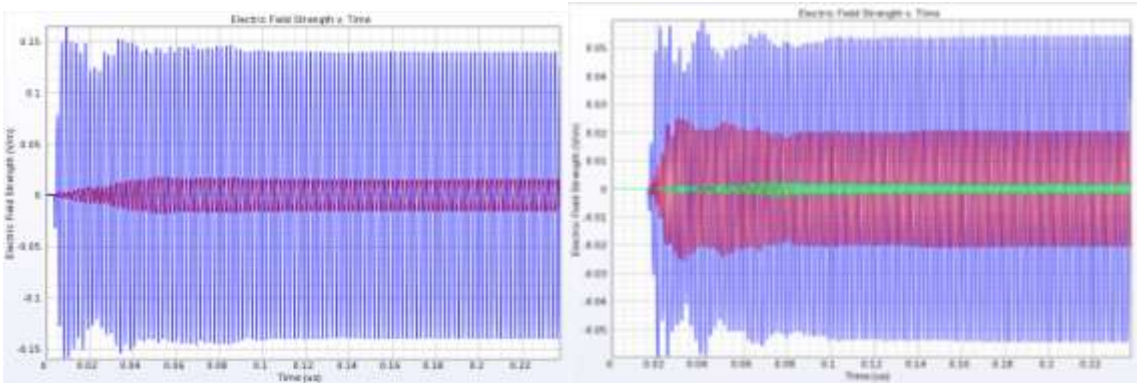

c) The XFDTD™ algorithm determines the field phasors by using the so-called "two-equations two-unknowns" method. Details of the algorithm are explained in [3].

9) Computing peak SAR from field components

a) The SAR for an individual voxel is computed according to the IEC/IEEE 62704-1 standard. In particular, the three components of the electric field are computed in the center of each voxel and then the SAR is computed as below:

$$SAR = \sigma_{voxel} \frac{|E_x|^2 + |E_y|^2 + |E_z|^2}{2\rho_{voxel}},$$

where σ_{voxel} and ρ_{voxel} are the conductivity and the mass density of the voxel.

10) One-gram and ten-gram averaged SAR procedures

a) XFDTD™ computes the Specific Absorption Rate (SAR) in each complete cell containing lossy dielectric material and with a non-zero material density. Using the SAR values computed for each voxel of the model the averaging calculation employs the method and specifications defined in the IEC/IEEE 62704-1 standard to generate one-gram and ten-gram average SAR.

11) Total computational uncertainty – We derived an estimate for the uncertainty of FDTD methods using the uncertainly budget defined in IEC/IEEE 62704-2-2017 standard. The details of uncertainty evaluation are provided in the Annex B.

In addition as discussed in 6(a), a conservative bias has been introduced in the evaluations so as to reduce concerns regarding the computational uncertainty related to the car modeling, antenna modeling, and phantom modeling.

12) Test results for determining SAR compliance

a) Illustrations showing the SAR distribution of dominant peak locations produced by the test transmitter, with respect to the phantom and test device, are provided in the SAR report.

b) The input impedance and the total power radiated under the impedance match conditions that occur at the test frequency are provided by XFDTD™. XFDTD™ computes the input impedance by following the method outlined in [4], which consists in performing the integration of the steady-state magnetic field around the feed point edge to compute the steady-state feed point current (*I*), which is then used to divide the feed-gap steady-state voltage (*V*). The net average radiated power is computed as

$$P_{XFDTD} = \frac{1}{2}\mathrm{Re}\left\{VI^*\right\}$$

Both the input impedance and the net average radiated power are provided by XFDTD™ at the end of each individual simulation.

We normalize the SAR to such a power, thereby obtaining SAR per radiated Watt (*normalized SAR*) values for the whole body and the 1-g SAR. Finally, we multiply such normalized SAR values times the max power rating of the device under test. In this way, we obtain the exposure metrics for 100% talk-time, i.e., without applying source-based time averaging.

c) For mobile radios, 50% source-based time averaging is applied by multiplying the SAR values determined at point 12(b) times a 0.5 factor.

d) The final SAR values used for compliance evaluation for each simulated configuration are obtained by applying the IEC/IEEE 62704-2-2017 standard adjustment factors to account for exposure variation in population.

REFERENCES

[1] K. S. Yee, "Numerical Solution of Initial Boundary Value Problems Involving Maxwell's Equations in Isotropic Media," *IEEE Transactions on Antennas and Propagation*, vol. 14, no. 3, 302-307, March 1966.

[2] C. M. Collins and M. B. Smith, "Calculations of B1 distribution, SNR, and SAR for a surface coil against an anatomically-accurate human body model," *Magn. Reson. Med*., 45:692-699, 2001. (enclosed TIF)

[3] C. M. Furse and O. P. Gandhi, "Calculation of electric fields and currents induced in a millimeter-resolution human model at 60 Hz using the FDTD method with a novel time-to-frequency-domain conversion**,"** Antennas and Propagation Society International Symposium, 1996.

[4] *The Finite Difference Time Domain Method for Electromagnetics*, Chapter 14.2, by K. S. Kunz and R. J. Luebbers, CRC Press, Boca Raton, Florida, 1993.

[5] *Validation of Mobile Antenna Modeling by Comparison with Near-field Measurements*," Report to the IEEE Standards Coordinating Committee 34, Sub-Committee 2, 2006.

[6] S. Gabriel, R. W. Lau, and C. Gabriel. 1996. The dielectric properties of biological tissues: III. Parametric models for the frequency spectrum of tissues. Phys. Med. Biol. 41:2271–2293.